Article

Exchange of Organic Radicals with Organo-Cobalt Complexes Formed in the Living Radical Polymerization of Vinyl Acetate

Shan Li, Bas de Bruin, Chi-How Peng, Michael Fryd, and Bradford B. Wayland

J. Am. Chem. Soc., **2008**, 130 (40), 13373-13381 • DOI: 10.1021/ja804010h • Publication Date (Web): 10 September 2008

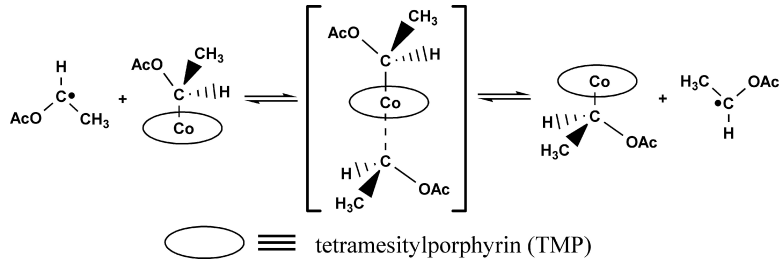

More About This Article

Additional resources and features associated with this article are available within the HTML version:

- Supporting Information
- Access to high resolution figures
- Links to articles and content related to this article
- Copyright permission to reproduce figures and/or text from this article

View the Full Text HTML

J|A|C|S
ARTICLES

Published on Web 09/10/2008

Exchange of Organic Radicals with Organo-Cobalt Complexes Formed in the Living Radical Polymerization of Vinyl Acetate

Shan Li,[†] Bas de Bruin,[‡] Chi-How Peng,[†] Michael Fryd,[†] and Bradford B. Wayland*,[†,§]

Department of Chemistry, University of Pennsylvania, Philadelphia, Pennsylvania 19104-6323, University of Amsterdam, Van't Hoff Institute for Molecular Sciences (HIMS), Department of Homogeneous and Supramolecular Catalysis, Nieuwe Achtergracht 166, 1018 WV Amsterdam, The Netherlands, and Department of Chemistry, Temple University, Philadelphia, Pennsylvania 19122

Received May 28, 2008; E-mail: wayland@sas.upenn.edu

Abstract: Exchange of organic radicals between solution and organo-cobalt complexes is experimentally observed and the reaction pathway is probed through DFT calculations. Cyanoisopropyl radicals from AIBN (2,2′-azobisisobutyronitrile) enter solutions of cobalt(II) tetramesityl porphyrin ((TMP)Co^{II}•, **1**) and vinyl acetate (VAc) in benzene and react to produce transient hydride (TMP)Co−H and radicals (•$CH(OAc)CH_2C(CH_3)_2CN$ (R_1•)) that proceed on to form organo-cobalt complexes (TMP)Co−$CH(OAc)CH_3$ (**4**, Co−R_2) and (TMP)Co−$CH(OAc)CH_2C(CH_3)_2CN$ (**3**, Co−R_1), respectively. Rate constants for cyanoisopropyl radical addition with vinyl acetate and hydrogen atom transfer to (TMP)Co^{II}• are reported through kinetic studies for the formation and transformation of organo-cobalt species in this system. Rate constants for near-degenerate exchanges of radicals in solution with organo-cobalt complexes are deduced from ^{1}H NMR studies and kinetic modeling. DFT computations revealed formation of an unsymmetrical adduct of (TMP)Co−$CH(OAc)CH_3$ (**4**) with •$CH(OAc)CH_3$ (R_2•) and support an associative pathway for radical interchange through a three-centered three-electron transition state [R···Co···R]. Associative radical interchange of the latent radical groups in organo-cobalt porphyrin complexes with freely diffusing radicals in solution that is observed in this system provides a pathway for mediation of living radical polymerization of vinyl acetate.

Introduction

Reactions of organic radicals with metallo-radicals and organometallic complexes have a central role in several pathways that mediate living radical polymerization (LRP)[1−16] and catalytic chain transfer (CCT).[17−21] The metal site reactions that occur when organic radicals interact with metal-centered radicals and organo-metal species in solution are shown in Scheme 1.[22,23] Interactions of organic radicals (•$C(CH_3)(R)X$) with metal-centered radicals (M•) in solution produce a solvent caged radical pair (M••$C(CH_3)(R)X$) which can collapse to form an organometallic complex (M−$C(CH_3)(R)X$), separate back into freely diffusing radicals (M• + •$C(CH_3)(R)X$), or react by M• abstracting a β-hydrogen from the radical (•$C(CH_3)(R)X$) to form a metal hydride (M−H) and an olefin (CH_2═$C(R)X$) (Scheme 1A).[22]

[†] University of Pennsylvania.
[‡] University of Amsterdam.
[§] Temple University.

(1) Wayland, B. B.; Poszmik, G.; Mukerjee, S. L.; Fryd, M. *J. Am. Chem. Soc.* **1994**, *116*, 7943–7944.
(2) Wayland, B. B.; Peng, C.-H.; Fu, X.; Lu, Z.; Fryd, M. *Macromolecules* **2006**, *39*, 8219–8222.
(3) Peng, C.-H.; Fryd, M.; Wayland, B. B. *Macromolecules* **2007**, *40*, 6814–6819.
(4) Peng, C.-H.; Scricco, J.; Li, S.; Fryd, M.; Wayland, B. B. *Macromolecules* **2008**, *41*, 2368–2373.
(5) Poli, R. *Angew. Chem., Int. Ed.* **2006**, *45*, 5058–5070.
(6) Maria, S.; Kaneyoshi, H.; Matyjaszewski, K.; Poli, R. *Chem.−Eur. J.* **2007**, *13*, 2480–2492.
(7) Debuigne, A.; Caille, J.-R.; Jèrôme, R. *Angew. Chem., Int. Ed.* **2005**, *44*, 1101–1104.
(8) Debuigne, A.; Willet, N.; Jèrôme, R.; Detrembleur, C. *Macromolecules* **2007**, *40*, 7111–7118.
(9) Debuigne, A.; Champouret, Y.; Jérôme, R.; Poli, R.; Detrembleur, C. *Chem.−Eur. J.* **2008**, *14*, 4046–4059.
(10) Kaneyoshi, H.; Matyjaszewski, K. *Macromolecules* **2005**, *38*, 8163–8169.
(11) Kaneyoshi, H.; Matyjaszewski, K. *J. Polym Sci. Part A: Polym. Chem.* **2007**, *45*, 447–459.
(12) Kato, M.; Kamigaito, M.; Sawamoto, M.; Higashimura, T. *Macromolecules* **1995**, *28*, 1721–1723.
(13) Wakioka, M.; Baek, K.-Y.; Ando, T.; Kamigaito, M.; Sawamoto, M. *Macromolecules* **2002**, *35*, 330–333.
(14) Asandei, A. D.; Moran, I. W. *J. Am. Chem. Soc.* **2004**, *126*, 15932–15933.
(15) Asandei, A. D.; Saha, G. *Macromolecules* **2006**, *39*, 8999–9009.
(16) Shaver, M. P.; Allan, L. E. N.; Gibson, V. C. *Organometallics* **2007**, *26*, 4725–4730.
(17) Gridnev, A. A.; Ittel, S. D. *Chem. Rev.* **2001**, *101*, 3611–3660.
(18) Li, Y.; Wayland, B. B. *Chem. Commun.* **2003**, 1594–1595.
(19) Tang, L.; Norton, J. R. *Macromolecules* **2006**, *39*, 8229–8235.
(20) Stoffelbach, F.; Poli, R.; Maria, S.; Richard, P. *J. Organomet. Chem.* **2007**, *692*, 3133–3143.
(21) Allan, L. E. N.; Shaver, M. P.; White, A. J. P.; Gibson, V. C. *Inorg. Chem.* **2007**, *46*, 8963–8970.
(22) Halpern, J. *Polyhedron* **1988**, *7*, 1483–1490.
(23) Ng, F. T. T.; Rempel, G. L.; Mancuso, C.; Halpern, J. *Organometallics* **1990**, *9*, 2762–2772.

Scheme 1. Reactions of Metal-Centered Radicals and Organo-Metal Complexes with Organic Radicals[a]

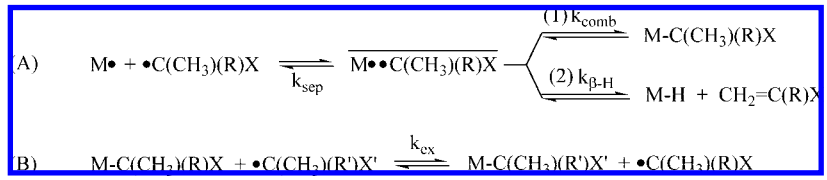

[a] (A) Reactions of organic radicals with metal-centered radicals relevant to control of radical polymerization. (B) Exchange of organic radicals with the organic units in organo-metal complexes.

Catalytic chain transfer (CCT) is associated with fast β-H abstraction by a metal-centered radical (M•) from the growing polymeric radical to form a metal hydride (M−H) (Scheme 1A2) that subsequently adds with the monomer to produce an organometallic complex (M−R). Reversible homolysis of the organo-metal bond in the absence of β-H transfer provides an organo-metal route to obtain living radical polymerization by a reversible termination (RT) mechanism (Scheme 1A1, eq 1).[2,24−26] When the exchange of freely diffusing radicals in solution with the dormant organic units in organometallic complexes is fast, then a LRP can occur by a degenerative transfer (DT) mechanism (Scheme 1B, eq 2).[4,27−29] Cobalt porphyrin complexes can achieve each of the reactions with organic radicals described in Scheme 1 and thus function as prototype systems to explore the pathways, potential scope, and limitation of living radical polymerization by both RT (Scheme 1A1) and DT (Scheme 1B) as well as CCT (Scheme 1A2).

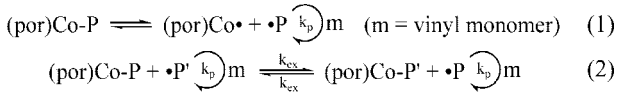

Degenerative transfer provides a convenient method to increase the polymerization rate and expand the scope of monomers in living radical polymerization mediated by organo-cobalt porphyrin complexes.[2−4] This article reports on the formation of organo-metal intermediates, hydrogen atom transfer, and radical exchange reactions that occur in the previously reported living radical polymerization (LRP) of vinyl acetate (VAc) mediated by organo-cobalt tetramesityl porphyrin complexes ((TMP)Co−R).[4] Precise control of LRP of vinyl acetate is challenging because of the high energy unstabilized radicals (•CH(OAc)R),[13,27,30−34] but mediation by cobalt acetylacetonate[7−9] and cobalt porphyrin complexes[4] are showing encouraging progress. Large equilibrium constants for organo-Co(TMP) complex formation with radicals derived from vinyl acetate (•CH(OAc)CH_2R) inhibit both catalytic chain transfer (CCT) and living radical polymerization by reversible termination (RT), but exchange of organic radicals between the solution and dormant organic radical units in organo-cobalt complexes provides a route for (TMP)Co-organo complexes to mediate living radical polymerization of VAc by a degenerative transfer (DT) mechanism.[4] Rate constants for near degenerate radical exchange of organic radicals with sixteen-electron organo-cobalt porphyrin complexes are experimentally evaluated and the nature of the reaction pathway probed using DFT calculations.

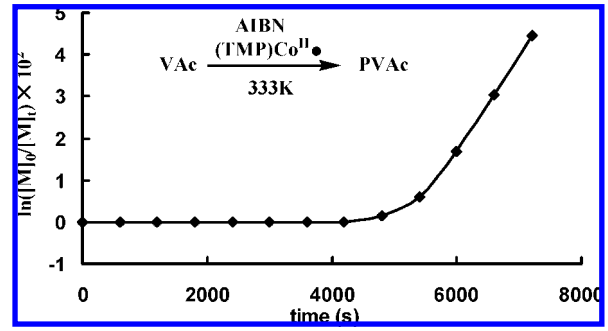

Figure 1. First order rate plot for vinyl acetate polymerization at 333 K mediated by cobalt tetramesitylporphyrin complexes using AIBN as the source of initiator radicals. Initial concentrations: $[(TMP)Co^{II}\bullet]_i = 4.31 \times 10^{-4}$ M, $[VAc]_i = 1.27$ M, $[AIBN]_i = 1.49 \times 10^{-2}$ M (At 7200 s: $M_n = 3340$, PDI = 1.16). (The quantity of radicals from AIBN entering solution as a function of time is given in Supporting Information).

Results and Discussion

Solutions of vinyl acetate (VAc), azo radical source (AIBN), and cobalt(II) tetramesityl porphyrin ($(TMP)Co^{II}\bullet$, **1**) when heated at 333K show an induction period followed by the on set of radical polymerization of VAc (Figure 1). A representative first order rate plot for the polymerization of VAc using AIBN as the external radical source for the cyanoisopropyl radical ($\bullet C(CH_3)_2CN$, **2**) in the presence of $(TMP)Co^{II}\bullet$ is shown in Figure 1. During the induction period prior to VAc polymerization, paramagnetic $(TMP)Co^{II}\bullet$ is converted to diamagnetic organo-cobalt porphyrin complexes and the time evolution is conveniently followed by changes in the porphyrin ^{1}H NMR (Figure 2a−c and Figure S1, Supporting Information). After the induction period cyanoisopropyl radicals (**2**) from AIBN continue to flow into the solution and the rate of VAc polymerization follows standard first order rate behavior ($\ln[M]_0/[M]_t = k_p[R\bullet]t$) where the slope of the first order rate plot is proportional to the square root of the AIBN concentration ($[R\bullet] = ((k_i/2k_t)[AIBN])^{1/2}$) (Figure 1). These characteristics are usually associated with regular uncontrolled radical polymerization, but the polymers formed in the cobalt porphyrin mediated

(24) Matyjaszewski, K.; Xia, J. H. *Chem. Rev.* **2001**, *101*, 2921–2990.
(25) Kamigaito, M.; Ando, T.; Sawamoto, M. *Chem. Rev.* **2001**, *101*, 3689–3746.
(26) Yoshikawa, C.; Goto, A.; Fukuda, T. *Macromolecules* **2003**, *36*, 908–912.
(27) Iovu, M. C.; Matyjaszewski, K. *Macromolecules* **2003**, *36*, 9346–9354.
(28) Chiefari, J.; Chong, Y. K.; Ercole, F.; Krstina, J.; Jeffery, J.; Le, T. P. T.; Mayadunne, R. T. A.; Meijs, G. F.; Moad, C. L.; Moad, G.; Rizzardo, E.; Thang, S. H. *Macromolecules* **1998**, *31*, 5559–5562.
(29) Moad, G.; Rizzardo, E.; Thang, S. H. *Aust. J. Chem.* **2005**, *58*, 379–410.
(30) Chamot, D.; Corpart, P.; Adam, H.; Zard, S. Z.; Biadatti, T.; Bouhadir, G. *Macromol. Symp.* **2000**, *150*, 23–32.
(31) Destarac, M.; Charmot, D.; Franck, X.; Zard, S. Z. *Macromol. Rapid Commun.* **2000**, *21*, 1035–1039.
(32) Rizzardo, E.; Chiefari, J.; Mayadunne, R.; Moad, G.; Thang, S. *Macromol. Symp.* **2001**, *174*, 209–212.
(33) Destarac, M.; Taton, D.; Zard, S. Z.; Saleh, T.; Six, Y. *ACS Symposium Series* **2003**, *854*, 536–550.
(34) Stenzel, M. H.; Cummins, L.; Roberts, G. E.; Davis, T. P.; Vana, P.; Barner-Kowollik, C. *Macromol. Chem. Phys.* **2003**, *204*, 1160–1168.

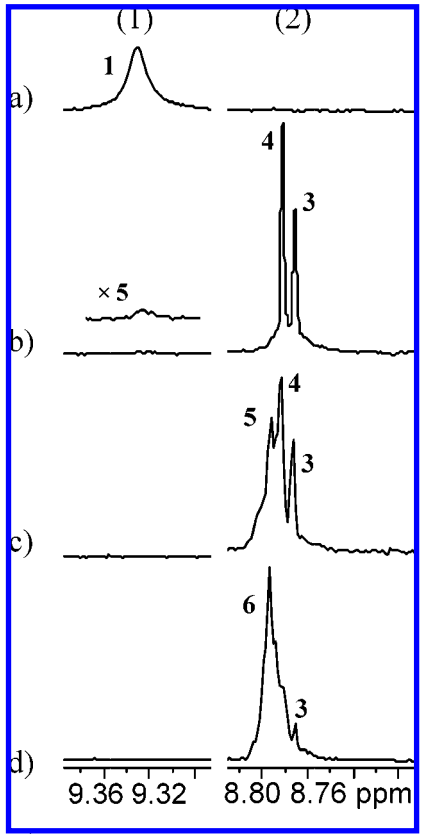

Figure 2. Changes in the porphyrin ^{1}H NMR (300 MHz) as a function of time through the induction period of VAc polymerization. (1) *m*-phenyl hydrogens of paramagnetic (TMP)Co^{II}•, (2) pyrrole hydrogens of diamagnetic organo-Co(TMP) complexes. Initial concentrations: $[(TMP)Co^{II}\bullet]_i = 4.31 \times 10^{-4}$ M, $[VAc]_i = 1.27$ M, $[AIBN]_i = 1.49 \times 10^{-2}$ M. Time (s) = (a) 0, (b) 3600, (c) 4200, (d) 5400. The organo-cobalt species are identified by the high-field ^{1}H NMR resonances for organic units attached to the cobalt center (Figure 3). Additional data on the changes in the porphyrin ^{1}H NMR during the induction period are provided in the Supporting Information (Figure S1).

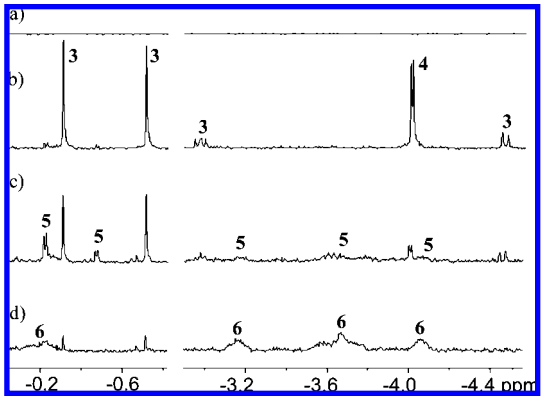

Figure 3. High field ^{1}H NMR (300 MHz) resonances for organo-cobalt species produced as a function of time in reactions of (TMP)Co^{II}•, AIBN, and vinyl acetate in C_6D_6 (333 K). Initial concentrations: $[(TMP)Co^{II}\bullet]_i = 4.31 \times 10^{-4}$ M, $[VAc]_i = 1.27$ M, $[AIBN]_i = 1.49 \times 10^{-2}$ M. (**3**) = (TMP)Co−CH(OAc)CH$_2$−C(CH$_3$)$_2$CN, (**4**) = (TMP)Co−CH(OAc)CH$_3$, (**5**) = (TMP)Co−CH(OAc)CH$_2$−CH(OAc)CH$_3$, (**6**) = (TMP)Co−CH(OAc)CH$_2$−CH(OAc)CH$_2$P. Time (s) = (a) 0, (b) 3600, (c) 4200, (d) 5400.

process increase linearly in molecular weight with conversion[4] and have relatively low polydispersities which are characteristics of a living radical polymerization.

Formation of the organometallic species during the course of the cobalt porphyrin mediated radical polymerization of vinyl acetate is followed by ^{1}H NMR changes in both the pyrrole hydrogen region ($\delta = 8.74-8.82$ ppm) and the high field region ($\delta = +0.5 \sim -5$ ppm) for organic groups attached to cobalt center (Figures 2, 3). Two organo-cobalt complexes (TMP)Co−CH(OAc)CH$_2$−C(CH$_3$)$_2$CN (**3**, Co−R$_1$) and (TMP)Co−CH(OAc)CH$_3$ (**4**, Co−R$_2$) appear during the early portion of the induction period when substantial concentrations of (TMP)Co^{II}• are present (eqs 3–6).

$$CH_2{=}CH(OAc) + \bullet C(CH_3)_2CN \quad (R\bullet) \rightarrow \bullet CH(OAc)CH_2{-}C(CH_3)_2CN \quad (R_1\bullet) \quad (3)$$

$$(TMP)Co^{II}\bullet + \bullet CH(OAc)CH_2{-}C(CH_3)_2CN \rightarrow (TMP)Co{-}CH(OAc)CH_2{-}C(CH_3)_2CN \quad (Co{-}R_1) \quad (4)$$

$$(TMP)Co^{II}\bullet + \bullet C(CH_3)_2CN \quad (R\bullet) \rightleftharpoons (TMP)Co{-}H + CH_2{=}C(CH_3)CN \quad (5)$$

$$(TMP)Co{-}H + CH_2{=}CH(OAc) \rightarrow (TMP)Co{-}CH(OAc)CH_3 \quad (Co{-}R_2) \quad (6)$$

Complexes **3** and **4** are formed by reaction pathways that compete for the cyanoisopropyl radical (•C(CH$_3$)$_2$CN, R•) that enters solution. When R• adds to monomer (CH$_2$=CH(OAc), VAc), a monomer-based radical •CH(OAc)CH$_2$−C(CH$_3$)$_2$CN (R$_1$•) is formed. Before R$_1$• can propagate further with monomers it combines with (TMP)Co^{II}• by a near diffusion controlled reaction to produce the organometallic complex (TMP)Co−CH(OAc)CH$_2$−C(CH$_3$)$_2$CN (**3**, Co−R$_1$). Appearance of **3** is easily identified by a pair of nearly equal intensity diastereotopic methyl resonances (δC(CH$_3$)$_2$CN = −0.30, −0.69 ppm) along with the diastereotopic C*H*$_2$ peaks (d of d, $\delta = -2.91$ ppm, $J_{1H\text{-}1H} = 14.2$ Hz, $J_{1H\text{-}1H} = 10.9$ Hz; d, $\delta = -4.40$ ppm, $J_{1H\text{-}1H} = 14.2$ Hz) (Figure 3). Another reaction pathway for cyanoisopropyl radicals (R•) that enter solution is β-H abstraction by (TMP)Co^{II}• to form a transient cobalt hydride (TMP)Co−H, which adds with a VAc monomer to produce the organometallic complex (TMP)Co−CH(OAc)CH$_3$ (**4**, Co−R$_2$). Formation of **4** in solution is readily followed by observation of a particularly characteristic high field methyl doublet ($\delta = -3.92$ ppm, $J_{1H\text{-}1H} = 5.3$ Hz), along with the −CH− quartet ($\delta = 0.48$ ppm, $J_{1H\text{-}1H} = 5.3$ Hz), and the acetate methyl singlet ($\delta = 0.080$ ppm) (Figure 3 and Supporting Information).

Addition of (TMP)Co−H to the double bond of vinyl acetate (eq 6) forms the Markovnikov product ((TMP)Co−CH(OAc)CH$_3$, **4**) as the exclusive species observed in the ^{1}H NMR. Concerted addition of (TMP)Co−H to CH$_2$=CH(OAc) is blocked by the porphyrin pyrrole nitrogen donors that occupy all of the *cis*-coordination sites adjacent to the Co−H unit. In benzene solvent medium the lowest energy stepwise pathway most likely involves hydrogen atom transfer to the olefin to give a radical pair that collapses to the organometallic complex.

$$(TMP)Co{-}H + CH_2{=}CH(OAc) \rightleftharpoons (TMP)Co^{II}\bullet \bullet CH(OAc)CH_3 \rightleftharpoons (TMP)Co{-}CH(OAc)CH_3$$

Kinetic preference for the Markovnikov product produced through a hydrogen atom transfer mechanism results from the relative stability of the two possible intermediate radicals •CH(OAc)CH$_3$ and •CH$_2$CH$_2$OAc. The enthalpy of isomerization from •CH(OAc)CH$_3$ to •CH$_2$CH$_2$OAc of +7 kcal mol^{-1}

Scheme 2. Reactions of Cyanoisopropyl Radicals with (TMP)Co^{II}• and Vinyl Acetate That Produce Organo-Cobalt Complexes during the Induction Period for Radical Polymerization of Vinyl Acetate Mediated by Organo-Co(TMP) Complexes

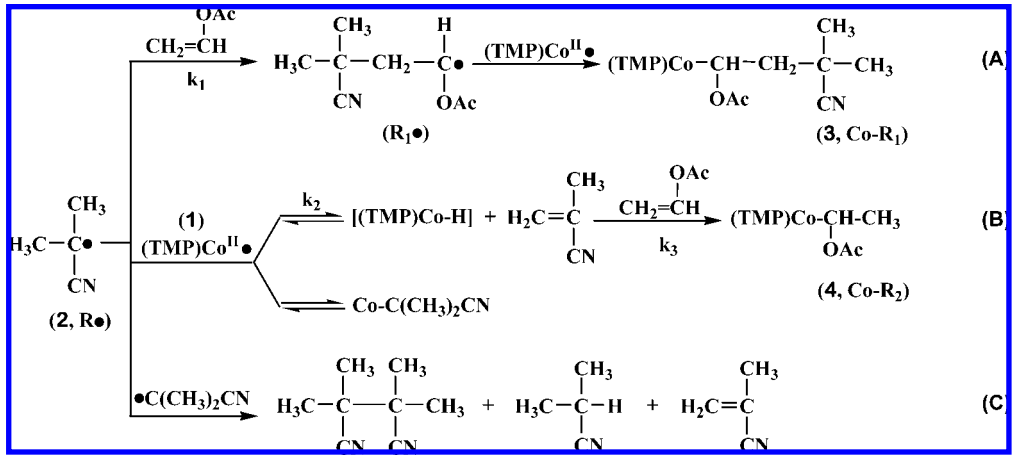

Scheme 3. Radical Propagation, Exchange, and Termination Processes Subsequent to the Induction Period

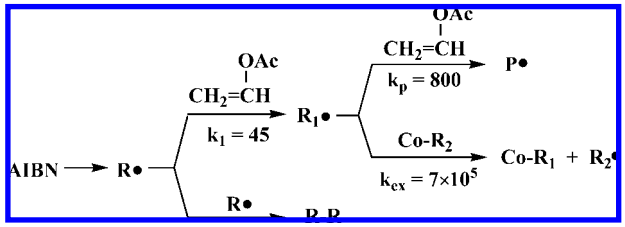

computed at the Gaussian B3LYP 6-31G(d) level[35] is consistent with the high selectivity for (TMP)Co−CH(OAc)CH$_3$. The initially formed kinetic product (TMP)Co−CH(OAc)CH$_3$ (**4**) is not observed to isomerize over extended periods of time in benzene and undoubtedly **4** is also the thermodynamic product. The polarity of organo-metal bonds (M^+R^-) provides an electronic effect that gives a thermodynamic preference for placing the electron withdrawing group on the α-carbon[36] and this electronic effect in this case more than compensates for the increased steric repulsion. (TMP)Co−CH(OAc)CH$_3$ is thus both kinetically and thermodynamically preferred to (TMP)Co−CH$_2$CH$_2$OAc.

Organo-cobalt complexes of vinyl acetate oligomers begin to form when (TMP)Co^{II}• is no longer detected in the ^{1}H NMR (Figure 2c, d). The initial oligomer complex that appears is (TMP)Co−CH(OAc)CH$_2$−CH(OAc)CH$_3$ (**5**, Co−R$_3$). Complex **5** corresponds to the insertion of one VAc monomer unit into the (TMP)Co−CH(OAc)CH$_3$ bond (eq 7) although the actual

$$\text{(TMP)Co}-\text{CH(OAc)CH}_3+\text{CH}_2{=}\text{CH(OAc)} \rightarrow \text{(TMP)Co}-\text{CH(OAc)CH}_2-\text{CH(OAc)CH}_3 \quad (7)$$

pathway undoubtedly involves sequential radical exchange and propagation events (eqs 8–12). Doublet methyl resonances (δ = −0.47, −0.22 ppm, $J_{1H\text{-}1H}$ = 6.4 Hz) are assigned to the terminal methyl groups for the diastereomers of **5** that result from two chiral carbon centers. When the organo-cobalt complexes **3** and **4** decrease in concentration as reflected by ^{1}H NMR intensities, the VAc oligomer and polymer complexes ((TMP)Co−CH(OAc)CH$_2$P, **6**) grow in intensity during and after the final stage of the induction period (Figures 2d, 3d). During this time period when (TMP)Co^{II}• has been fully converted to **3** and **4** the redistribution of organo-cobalt complexes must result from exchange of radicals in solution with the organic units in organometallic complexes (R′• + Co−R ⇌ R′−Co + R•) (eqs 8–12).

$$\text{R}\bullet + \text{VAc} \rightarrow \text{R}_1\bullet \quad (8)$$

$$\text{R}_1\bullet + \text{Co}-\text{R}_2 \rightleftharpoons \text{Co}-\text{R}_1 + \text{R}_2\bullet \quad (9)$$

$$\text{R}_2\bullet + \text{VAc} \rightarrow \text{R}_3\bullet \quad (10)$$

$$\text{R}_3\bullet + \text{Co}-\text{R}_1 \rightleftharpoons \text{Co}-\text{R}_3 + \text{R}_1\bullet \quad (11)$$

$$\text{R}_3\bullet + \text{Co}-\text{R}_2 \rightleftharpoons \text{Co}-\text{R}_3 + \text{R}_2\bullet \quad (12)$$

Scheme 2 outlines the reactions that occur in the polymerization system containing (TMP)Co^{II}•, AIBN, and VAc during the early stage when substantial quantities of (TMP)Co^{II}• remain. Cyanoisopropyl radicals (**2**) experience a series of competitive reactions in the system containing (TMP)Co^{II}• and vinyl acetate which include initiating VAc polymerization, forming a weakly bonded organo-cobalt complex, β-H transfer to form (TMP)Co−H, and radical termination (Scheme 2).

The cyanoisopropyl radical (**2**) adds to the VAc monomer and initiates the propagation of VAc oligomer radicals. During the induction period only one propagation event occurs to form •CH(OAc)CH$_2$−C(CH$_3$)$_2$CN (R$_1$•) which rapidly combines with (TMP)Co^{II}• to give (TMP)Co−CH(OAc)CH$_2$−C(CH$_3$)$_2$CN (**3**, Co−R$_1$). The cyanoisopropyl radical (**2**) alternately reacts with (TMP)Co^{II}• either to form the organometallic complex (TMP)-Co−C(CH$_3$)$_2$CN or to produce a cobalt hydride ((TMP)Co−H) by β-H abstraction from **2**. These two reactions are the general reactions between organic radicals and metal-centered radicals shown in Scheme 1(A). The highly stabilized and sterically demanding •C(CH$_3$)$_2$CN radical forms a weakly bonded organometallic complex Co−C(CH$_3$)$_2$CN (K(333K) ≈ 5 × 10^6, ΔH^o = −17 kcal mol^{-1})[37] that is highly dissociated at 333K and thus does not have an important role in the overall process. The cobalt hydride reacts rapidly with VAc olefin monomer by exclusive Markovnikov addition to form (TMP)Co−CH-(OAc)CH$_3$ (**4**, Co−R$_2$). Organo-cobalt complexes **3** and **4** have

(35) Calculations were performed using Gaussian B3LYP 6-31G(d) and the calculated energies are listed in Supporting Information. Computational support was provided by the National Science Foundation CRIF program, Grant CHE-0131132.

(36) Harvey, J. N. *Organometallics* **2001**, *20*, 4887–4895.

(37) Woska, D. C.; Xie, Z. D.; Gridnev, A. A.; Ittel, S. D.; Fryd, M.; Wayland, B. B. *J. Am. Chem. Soc.* **1996**, *118*, 9102–9109.

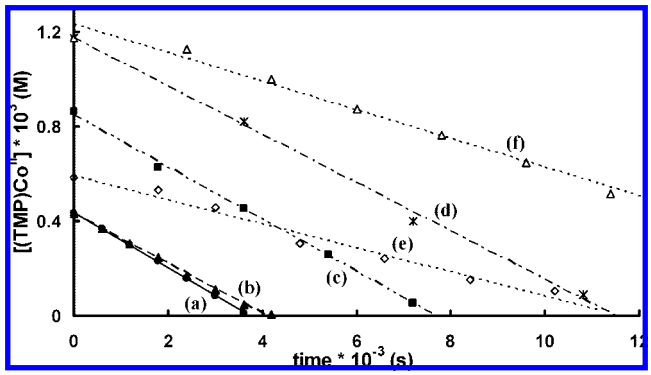

Figure 4. Time dependence for the molar concentration of (TMP)Co^{II}• in benzene solutions of (TMP)Co^{II}•, AIBN, and VAc (T = 333 K). $[AIBN]_i$: (a−d) = 1.49×10^{-2} M, (e, f) = 0.745 M. (Slope × 10^6 ($M\ s^{-1}$) = −d[(TMP)Co^{II}•]/dt: (a) −0.1178, (b) −0.1044, (c) −0.1104, (d) −0.1021, (e) −0.0508, (f) −0.0531). Initial conditions: (a) $[(TMP)Co^{II}•]_i = 4.31 \times 10^{-4}$ M, $[VAc]_i$ = 1.27 M; (b) $[(TMP)Co^{II}•]_i = 4.31 \times 10^{-4}$ M, $[VAc]_i$ = 0.637 M; (c) $[(TMP)Co^{II}•]_i = 8.63 \times 10^{-4}$ M, $[VAc]_i$ = 0.637M; (d) $[(TMP)Co^{II}•]_i = 1.17 \times 10^{-3}$ M, $[VAc]_i$ = 0.130M; (e) $[(TMP)Co^{II}•]_i = 5.86 \times 10^{-4}$ M, $[VAc]_i$ = 1.732M; (f) $[(TMP)Co^{II}•]_i = 1.17 \times 10^{-3}$ M, $[VAc]_i$ = 0.0217 M.

large equilibrium constants for formation (K(333K) > 10^{14}) and thus accumulate during the induction period. The final inevitable reaction for radical **2** is termination through bimolecular radical coupling or disproportionation (Scheme 2C).

During the time period when (TMP)Co^{II}• can be observed by ^{1}H NMR there is very little radical termination through bimolecular coupling. Effectively all of the cyanoisopropyl radicals either react with (TMP)Co^{II}• which ultimately produces (TMP)Co−CH(OAc)CH_3 (**4**, Co−R_2) or combine with the monomer (CH_2═CH(OAc)) which ultimately gives (TMP)-Co−CH(OAc)CH_2−C$(CH_3)_2$CN (**3**, Co−R_1) (Scheme 2). Over the range of VAc, AIBN, and (TMP)Co concentrations studied the rate of disappearance of (TMP)Co^{II}• has a first order dependence on the molar concentration of AIBN (−d[(TMP)-Co^{II}•]/dt = k_i[AIBN]) and is equal to the rate at which the cyanoisopropyl radical enters solution (Figure 4). These kinetic results experimentally demonstrate that effectively all of the radicals **2** that enter solution experience fast reactions that convert (TMP)Co^{II}• into organo-cobalt complexes (Schemes 2A, B). The induction period prior to the polymerization of VAc is determined by the time required to produce one equivalent of freely diffusing radicals per equivalent of (TMP)Co^{II}• which is proportional to the ratio of the initial concentrations of (TMP)-Co^{II}• to AIBN (Figure 4).

Two competing pathways convert (TMP)Co^{II}• into organo-cobalt complexes as shown in Scheme 2A, B, and the ratio of the molar concentration of (TMP)Co−CH(OAc)CH_2−C$(CH_3)_2$-CN (**3**) to (TMP)Co−CH(OAc)CH_3 (**4**) is observed to increase linearly as the ratio of the concentration of VAc to (TMP)Co^{II}• increases while holding the other concentrations constant (Figure S3, S4, Supporting Information). The ratio of the molar concentrations of **3** to **4** is accurately fitted to the ratio of their rate expressions ([**3**]/[**4**]) = (k_1[R•][VAc]/k_2[Co•][R•] = (k_1/k_2)([VAc]/[Co•]) which provides an accurate value for the ratio of k_1 to k_2 (($k_1/k_2)_{(333K)}$ = 9.0×10^{-5}).

The rate of formation of (TMP)Co−CH(OAc)CH_3 (**4**) is observed to be independent of the concentration of vinyl acetate over the range of concentrations studied ($[VAc]_i$ = 0.02−1.27 M) and thus the rate constant for reaction of (TMP)Co−H with VAc must be sufficiently large (k_3(333 K) > 200 $M^{-1}\ s^{-1}$) such that the rate of formation of **4** equals the rate of formation of

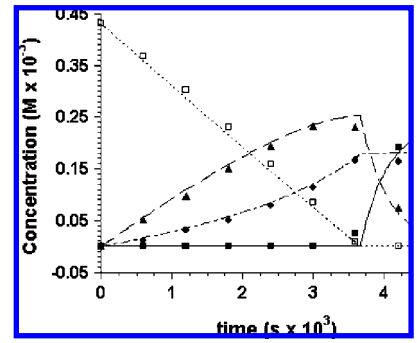

Figure 5. Experimental points and calculated lines for the concentrations of (TMP)Co^{II}• and (TMP)Co-organo complexes during the induction period. □ = (TMP)Co^{II}•, ● = (TMP)Co−CH(OAc)CH_2−C$(CH_3)_2$CN, ▲ = (TMP)Co−CH(OAc)CH_3, ■ = (TMP)Co−CH(OAc)CH_2−CH(OAc)CH_3. Initial concentrations: $[AIBN]_i = 1.49 \times 10^{-2}$ M, $[(TMP)Co^{II}•]_i = 4.31 \times 10^{-4}$ M, $[VAc]_i$ = 1.27 M. Parameters used in the kinetic simulations for reactions at 333 K are given in the Supporting Information.

(TMP)Co−H (d[(TMP)Co−H]/dt = d[**4**]/dt). Because the rate of formation of (TMP)Co−CH(OAc)CH_2−C$(CH_3)_2$CN (**3**) is first order in VAc, the ratio of **3** to **4** increases directly as the concentration of VAc increases.

Reactions of the cyanoisopropyl radical (**2**) and radical exchange processes that occur immediately following the induction period are shown in Scheme 3. After effectively all of the (TMP)Co^{II}• (**1**) is converted to organometallic complexes **3** and **4**, cyanoisopropyl radicals (**2**) from AIBN continue to flow into solution. During this time period the reactions of radical **2** are limited to combining with the vinyl acetate monomer to form R_1• (eq 8) and bimolecular termination (Scheme 3). The •C(CH_3)CN radical is highly stabilized and forms only a weakly bonded organo-cobalt complex with (TMP)Co^{II}•[37] and is not expected to be effective in exchanging with the much more strongly bonded organo-cobalt complexes derived from the higher energy vinyl acetate radicals (•CH(OAc)CH_2P). The kinetics for evolution of the organo-cobalt species subsequent to the conversion of (TMP)Co^{II}• to organo-cobalt complexes become dependent on both the rate constant for reaction of the cyanoisopropyl radical (**2**, R•) with VAc (k_1) (d[R_1•]/dt = k_1[R•][VAc]) and rate constants for exchange of radicals in solution with the latent radical units in organo-Co(TMP) complexes (R_m• + (TMP)Co−R_n ⇌ R_m−Co(TMP) + R_n•). The observed interconversion of organo-cobalt complexes (Co−R_1, Co−R_2, Co−R_3 ..., Co−R_n) after (TMP)-Co^{II}• has reacted away must result from these radical exchange processes.

The redistribution of organo-cobalt species after disappearance of (TMP)Co^{II}• (Figures 3, 5) provides experimental observations that illustrate the radical exchange process. The R_1• radicals produced from R• and VAc could propagate further with VAc to form oligomer radicals (P•) or exchange with the dormant organo-radical groups bound to cobalt in (TMP)Co−CH(OAc)CH_3 (**4**, Co−R_2). Decrease in concentration and ultimate disappearance of (TMP)Co−CH(OAc)CH_3 (**4**, Co−R_2) is ascribed to a near degenerate radical interchange between freely diffusing R_1• radicals in solution and the cobalt bound R_2 group (eq 9). Concomitant with the decline in Co−R_2 (**4**) is the appearance and growth of (TMP)Co−CH(OAc)CH_2CH-(OAc)CH_3 (**5**, Co−R_3). The only possible source of Co−R_3 (**5**) is from the R_2• radicals released from Co−R_2 propagating once with VAc (eq 10) to form R_3• (•CH(OAc)CH_2CH(OAc)CH_3) which then exchanges with Co−R_1 and Co−R_2 (eq 11, 12).

The terminal methyl group in (TMP)Co−CH(OAc)CH_3) (**4**, Co−R_2) comes from addition of (TMP)Co−H to CH_2=CH(OAc) regioselectively to form (TMP)Co−CH(OAc)CH_3 (eq 6). This is the exclusive route that produces a terminal methyl group and thus must also be the source for the terminal methyl of the R_3 group in (TMP)Co−CH(OAc)CH_2CH(OAc)CH_3 (**5**, Co−R_3).

Quantitative evaluation of the evolution and redistribution of (TMP)Co species (**1**, **3**, **4**, **5**) with time for a representative polymerization process with initial concentrations of [(TMP)-Co^{II}•]$_i$ = 4.31 × 10^{-4} M, [AIBN]$_i$ = 1.49 × 10^{-2} M, and [VAc]$_i$ = 1.27 M is shown in Figure 5. The kinetic simulations[38] shown in Figure 5 use a full kinetic model based on Scheme 2 and eqs 8−12. The set of reactions and corresponding rate constants used in the kinetic simulations are listed in the Supporting Information. At the early stage of the induction period, complexes **3** and **4** are produced concomitant with the decrease of the (TMP)Co^{II}• concentration. The distribution of **3** and **4** depends on the relative rates of radical addition to monomer (eq 3) and hydrogen atom transfer (eq 5) (Figure 5, S3, Supporting Information). During the final stage of the induction period when (TMP)Co^{II}• concentration is approaching zero, the oligomer-cobalt complex (TMP)Co−CH(OAc)CH_2CH-(OAc)CH_3 (**5**) begins to appear. The formation and distribution of each organometallic species are determined by the relative rates of monomer propagation and radical interchange (Figure 5, S3, Supporting Information).

The observed kinetics for disappearance of (TMP)Co^{II}• to form (TMP)Co−CH(OAc)CH_2−C$(CH_3)_2$CN (**3**, Co−R_1) and (TMP)Co−CH(OAc)CH_3 (**4**, Co−R_2) (−d[(TMP)Co^{II}•]/dt = k_1[R•][VAc] + k_2[R•][(TMP)Co^{II}•]) for a series of concentrations of VAc and (TMP)Co^{II}• provide an accurate evaluation of the ratio of k_1 to k_2 ((k_1/k_2) = 9.0 ± 0.2 × 10^{-5}). Kinetic simulations shown in Figure 5 were carried out by holding the ratio of k_1/k_2 (9.0 × 10^{-5}) constant while varying the absolute value for k_1 and k_2 and the rate constants for radical exchange such as k_9, k_{11}, k_{12}. The observed time dependencies for the concentrations of **3** and **4** could only be reasonably simulated when the absolute value for k_1 was relatively small compared to k_p(VAc) (~800 M^{-1} s^{-1}) and with rate constants for radical exchange greater than 7 × 10^5 M^{-1} s^{-1}. The best fit (333 K) shown as the lines in Figure 5 was obtained when k_1 = 45 M^{-1} s^{-1}, k_2 = 5 × 10^5 M^{-1} s^{-1} and radical exchange rate constants $k_9 = k_{12} \approx$ 7 × 10^5 M^{-1} s^{-1} and $k_{11} \approx$ 5 × 10^6 M^{-1} s^{-1}.

Confidence in the reliability of the kinetic analysis is obtained by the similarity of the derived hydrogen atom transfer rate constant (k_2(333 K) ≈ 5 × 10^5 M^{-1} s^{-1}) and the value of 4 × 10^5 M^{-1} s^{-1} reported for hydrogen transfer from methacrylonitrile oligomer radicals to cobalt(II) tetraphenyl porphyrin.[17,39] The radical exchange rates are not uniquely determined by the kinetic analysis, but reasonable fits of experimental data are only obtained when the rate constants for near degenerate radical interchange like eqs 9 and 12 are greater than 4 × 10^5 M^{-1} s^{-1} and less than 1 × 10^6 M^{-1} s^{-1}. The fit between experiment and calculation given in Figure 5 is obtained when the radical exchange rate constants k_9 and k_{12} are equal to 7 × 10^5 M^{-1} s^{-1}. The rate constants deduced for radical exchange (k_{ex}(333 K) ≈ 7 × 10^5 M^{-1} s^{-1}) (R_m• + (TMP)Co−R_n ⇌ R_m−Co(TMP) + R_n•) in the (TMP)Co system are comparable to or larger than the values reported for exchange rates of radicals with dithioesters (RAFT)[29,40] and a series of organo main group species[41−43] that are observed to control living radical polymerization by degenerative transfer. The observed radical exchange rate constants for the organo-Co(TMP) system (k_{ex}(333K) ≈ 7 × 10^5 $M^{-1}s^{-1}$) are large enough to account for obtaining relatively low polydispersities in the LRP of VAc mediated by organo-cobalt complexes (Figure 1).[4]

DFT Calculations. The process of radicals in solution interacting with organo-cobalt complexes and exchanging organo-groups was further investigated using DFT calculations to probe the reaction pathway. The degenerate exchange (ΔG^o = 0) of the 1-ethylacetate radical (•CH(OAc)CH_3, R_2•) derived by addition of a hydrogen atom to vinyl acetate with the corresponding organo-cobalt porphyrin complex ((TMP)Co−CH(OAc)CH_3, (TMP)Co−R_2) was chosen to emulate the near degenerate ($\Delta G^o \approx 0$) radical exchange reactions proposed to occur in the living radical polymerization system consisting of (TMP)Co^{II}•, AIBN, and VAc. An unsubstituted porphyrin ligand (por) was chosen as a computational model for the much larger tetramesityl porphyrin ligand (TMP) used in the experimental studies.

Both dissociative and associative pathways for radical exchange were computed. Particular interest was placed on examining the associative pathway for possible intermediates and redox processes involving the metal and porphyrin units such as the entering radical oxidizing the cobalt(III) porphyrin unit to give a coordinated carbanion and Co^{IV} ((por)$Co^{IV}(R_2)_2$) or porphyrin cation radical species ((por)$^{+\bullet}Co^{III}(R_2)_2$). The minimum energy structure and spin density plots for (por)-$Co(R_2)_2$ are shown in Figure 6. A summary of several of the more important computational results is given in Scheme 4.

The calculated dissociative pathway corresponding to Co−C bond homolysis is endergonic by +23 kcal mol^{-1}. This value is probably slightly overestimated, because the process involves a change of the spin state from singlet to two separated doublet states. The BP86 level of theory tends to underestimate the relative stability of radicals compared to closed-shell systems, but deviations from experimental values are usually smaller compared to the overestimated stability of radicals at the b3-lyp level of theory[44] and thus the hybrid HF-DFT functional b3-lyp tends to underestimate Co−ligand interactions.[45] For those reasons, the pure DFT functional BP86 is most probably

(38) The simulation program, MacKinetics v0.9.1, was generously provided by Dr. Walter S. Leipold III.

(39) Gridnev, A. A.; Ittel, S. D. *Macromolecules* **1996**, *29*, 5864–5874.

(40) Goto, A.; Sato, K.; Tsujii, Y.; Fukuda, T.; Moad, G.; Rizzardo, E.; Tang, S. H. *Macromolecules* **2001**, *34*, 402–498.

(41) Kwak, Y.; Goto, A.; Fukuda, T.; Kobayashi, Y.; Yamago, S. *Macromolecules* **2006**, *39*, 4671–4679.

(42) Goto, A.; Ohno, K.; Fukuda, T. *Macromolecules* **1998**, *31*, 2809–2814.

(43) Kwak, T.; Goto, A.; Fukuda, T.; Yamago, S.; Ray, B. Z. *Phys. Chem.* **2005**, *219*, 283–293.

(44) Hybrid HF/DFT functionals (such as b3-lyp) tend to overestimate the relative stability of radicals compared to closed-shell systems: (a) Saeys, M.; Reyniers, M.-F.; Marin, G. B.; Van Speybroeck, V.; Waroquier, M. *J. Phys. Chem. A* **2003**, *107*, 9147–9159. (b) Sustmann, R.; Sicking, W.; Huisgen, R. *J. Am. Chem. Soc.* **2003**, *125*, 14425–14434. (c) Jensen, K. P.; Ryde, U. *J. Phys. Chem. A* **2003**, *107*, 7539–7545. (d) Gosh, A. *J. Biol. Inorg. Chem.* **2006**, *11*, 712–724.

(45) Hybrid HF/DFT methods (such as b3-lyp) tend to underestimate the transition metal-ligand bond strengths. Deviations from experimental values are generally smaller for pure DFT methods (such as BP86): (a) Harvey, J. N. *Annu. Rep. Prog. Chem., Sect. C* **2006**, *102*, 203–226. (b) Schultz, N. E.; Zhao, Y.; Truhlar, D. G. *J. Phys. Chem. A* **2005**, *109*, 11127–11143. (c) Furche, F.; Perdew, J. P. *J. Chem. Phys.* **2006**, *124*, 044103/1−044103/27. (d) Waller, M. P.; Braun, H.; Hojdis, N.; Bühl, M. *J. Chem. Theory Comput.* **2007**, *3*, 2234–2242. See also refs 44c and 44d.

Figure 6. Optimized geometry (A) and spin density plot (B) for (porphine)Co(CH(OAc)CH$_3$)$_2$ (**7**).

Scheme 4. DFT (BP86/SV(P)) Calculated Standard Relative Free Energies (kcal mol^{-1}), Enthalpies (kcal mol^{-1}), Entropies (e.u.), and Bond Length Changes Corresponding to Dissociative Vinylacetyl Radical Dissociation from (Porphine)Co-R$_2$ and Associative Radical Exchange via (Porphine)Co(R$_2$)$_2$[a]

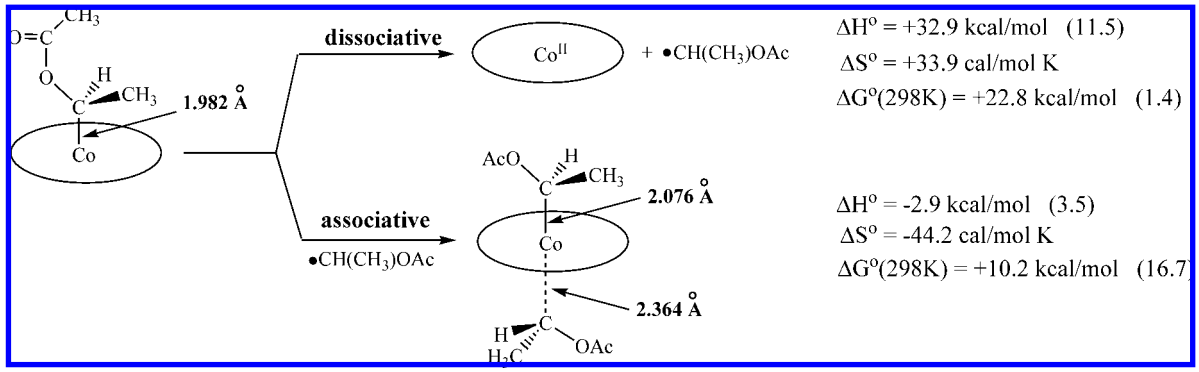

[a] Values in brackets are based on b3-lyp/TZVP single point calculations.

the better choice for the reactions under consideration in this paper. Single point b3-lyp level calculations produced ΔG° values that are too small for the dissociative pathway and too large for the associative pathway (Scheme 4). The associative pathway does not involve a spin change, and the relative energies computed using the BP86 level should be reliable. Formation of (por)Co(R$_2$)$_2$ by interaction of the 1-ethylacetate radical (R$_2$•) with the porphyrin cobalt-1-ethylacetyl organometallic complex (por)Co−R$_2$ is endergonic by +11.8 kcal mol^{-1} at 333 K (10.2 kcal mol^{-1} at 298 K) which is in good agreement with the experimental results. The DFT calculations are thus most consistent with the radical exchange occurring by an associative rather than a dissociative pathway (Scheme 4). The computed enthalpy change for the formation of (por)Co(R$_2$)$_2$ from (por)Co(R$_2$) and R$_2$• is slightly exothermic($\Delta H^{\circ} = -2.9$ kcal mol^{-1}). Optimization of separated (por)Co(R$_2$) and R$_2$• species and (por)Co(R$_2$)$_2$ resulted in a minimum energy structure (Figure 6, Scheme 4). Constraint geometry optimizations with longer Co−C bonds only led to higher energies (see Figure S5, Supporting Information, for the energy profile). The most important factor contributing to the barrier for the radical exchange is the entropy required to bring together the organic radical and alkyl-cobalt complex. The unsymmetrical adduct with two R$_2$ units (por)Co(R$_2$)$_2$ (**7**) is slightly stabilized by enthalpy (−2.9 kcal mol^{-1}) but is highly destabilized by entropy ($\Delta S^{\circ} = -44$ cal K^{-1} mol^{-1}; $-T\Delta S^{\circ}$(298 K) = +13.1 kcal mol^{-1}) (Scheme 4). In solution (condensed phase), the negative entropy term associated with bringing together (por)Co(R$_2$) and R$_2$• is probably smaller than obtained from our gas-phase DFT calculations, primarily due to a restriction of the translational degrees of freedom by conversion into other lattice modes, and possible contributions of solvation entropy terms, both of which are difficult to estimate by computational methods. This level of computation is thus expected to overestimate the activation barrier.

Purely based on the electronic energy optimizations, the structure of (por)Co(R$_2$)$_2$ given in Figure 6 is a minimum enthalpy structure and not a transition state (TS). In order to find an authentic transition state the free energy landscape would need to be computationally searched. It is probable that the true transition state is energetically close to that of **7** and having equal Co−C distances, for which the barrier to formation is mostly based on entropy.[46] The experimental barrier estimated from the measured rate constant at 333 K ($\Delta G^{\ddagger}_{exp} \approx +12$ kcal mol^{-1}) is close to the calculated ΔG° (+11.8 kcal mol^{-1}) for formation of radical adduct (**7**). Although this level of agreement must in part be fortuitous because transition state theory usually becomes less reliable for low barrier process.[47] The calculated energy profile for the process of moving from the unsymmetrical structure (**7**) to a structure with equal Co−C distances is both insensitive to distance and very small (Figure S7, Supporting Information), with an estimated contribution to the barrier for radical exchange of only about 0.2 kcal mol^{-1}. No real transition states could be located on the electronic energy surface by

(46) With the applied static DFT methods, there exist no methods to find transition states which exist only in the free energy landscape, but not in the electronic energy landscape. A way to treat such problems correctly would be Car-Parrinello molecular dynamics, which is beyond the scope of this article.

(47) Varandas, A. J. C.; Caridade, P. J. S. B.; Zhang, J. Z. H.; Qui, Q.; Han, K. L. *J. Chem. Phys.* **2006**, *125* (6), 064312/1−064312/11. (b) Troe, J. Z. *Phys. Chem.* **2004**, *218* (4), 457–467.

geometry optimizations, which is to be expected for low barrier processes dominated by entropy.[46]

The computations suggest that radical exchange occurs by a concerted radical interchange (S_H2) without either a cobalt(IV) or porphyrin$^{+\bullet}$ cation radical species on the reaction pathway. The computed path is essentially a concerted three-centered three orbital three electron process (S_H2) where the unpaired electron occupies a nonbonding molecular orbital with predominant contributions from the entering and leaving radical carbon centers and very little cobalt porphyrin character (Figure 6). It is the entropy change (-44 cal K^{-1} mol^{-1}) in forming the adduct structure that dominates the free energy barrier for exchanging the organo groups ($R_2\bullet + Co-R_2 \rightleftharpoons R_2-Co + R_2\bullet$).

As the radical from solution ($\bullet CH(OAc)CH_3$, $R_2\bullet$) interacts with the organo-metal complex the Co−C bond *trans* to the incoming radical increases from 1.982 Å to 2.076 Å in complex **7** and thus complex **7** contains one long (2.364 Å) and one short (2.076 Å) Co−C distance (Scheme 4). The spin density plot for **7** clearly illustrates that the unpaired electron predominantly resides at the 'radical carbon unit' with the longer Co−C distance, but there is also a substantial spin density on the 'alkyl carbon unit' with the shorter Co−C distance. The complex has negligible spin density on the cobalt porphyrin unit (Figure 6). This is just what is expected for a three-orbital three-electron cobalt(III) complex of one carbanion and one radical ($R\bullet\ Co^{III}$ **:**R). This is also the type of species that would occur on the reaction path for a second order homolytic substitution (S_H2) process. Related transfer of an organo group (R•) from an organo-cobalt complex (Co−R) to a cobalt(II) complex (Co•) by an S_H2 pathway (Co−R$\cdots\bullet$Co) is well-known.[48−51]

Organic radical exchange has recently been recognized as an important route to living radical polymerization mediated by a series of organo-main group compounds.[27,41,43,52,53] Radical exchange at transition metal centers of organometallic complexes has been recognized as a potentially significant process,[54−56] but direct observations of radical exchange are lacking. The probable role of radical exchange in producing low polydispersity polymers in living radical polymerizations mediated by cobalt[1−9] and titanium complexes[14,15] has been proposed, but the results presented in this article are to the best of knowledge the most direct observations and measurements of rate constants of radical exchange for organo-transition metal complexes.

Summary

Benzene solutions of $(TMP)Co^{II}\bullet$, AIBN, and vinyl acetate when heated at 333 K produce hydride (TMP)Co−H and radical $\bullet CH(OAc)CH_2C(CH_3)_2CN$ which then adds to VAc monomer or couples with $(TMP)Co^{II}\bullet$ to form organo-cobalt complexes (TMP)Co−CH(OAc)CH_3 and (TMP)Co−CH(OAc)CH_2C-$(CH_3)_2$CN, respectively. Kinetic studies (333 K) for the formation and transformation of organo-cobalt species in this system are used to derive rate constants for hydrogen atom transfer (5×10^5 M^{-1} s^{-1}), reaction of cyanoisopropyl radical with VAc (45 M^{-1} s^{-1}), and interchange of organic radicals in solution with the latent radical groups in organo-cobalt complexes (7×10^5 M^{-1} s^{-1}). DFT computations revealed formation of an unsymmetrical adduct of (TMP)Co−CH(OAc)CH_3 with $\bullet CH(OAc)CH_3$ and support an associative pathway for radical interchange through a three-centered three-electron transition state [R$\cdots$Co$\cdots$R]. The *in situ* generation of organo-cobalt complexes from Co(II) and the fast radical interchange of organo-cobalt porphyrin complexes with freely diffusing radicals in solution provides a degenerative transfer pathway for mediation of living radical polymerization of vinyl acetate.

Experimental Section

Materials. Vinyl acetate (Fluka, 99.0%, 0.0015% hydroquinone inhibitor) was stored at 4 °C and vacuum distilled at room temperature before use. The azo initiator, 2,2′-azobisisobutyronitrile (AIBN, $((CH_3)_2(CN)C)_2N_2$), was purchased from Aldrich (98%) and recrystallized from ethanol before use.[57] Cobaltous acetate ($Co(CH_3COO)_2\bullet 4H_2O$) and benzene-$D_6$ (D, 99.5%) were purchased from Fisher Scientific and Cambridge Isotope Laboratories, Inc., respectively, and used as received. Tetramesitylporphyrin $(TMP)H_2$ and cobalt(II)tetramesitylporphyrin ($(TMP)Co^{II}\bullet$) were synthesized following literature methods.[37,58]

Polymerization. Aliquots of solutions of $(TMP)Co^{II}\bullet$ and AIBN in C_6D_6 were mixed in a vacuum-adapted NMR tube and VAc was subsequently injected into the tube containing $(TMP)Co^{II}\bullet$ and AIBN. The solution was thoroughly mixed and then subjected to three freeze−pump−thaw cycles to remove the dissolved oxygen gas. ^{1}H NMR was run for the freshly degassed solution and recorded at the reaction profile as time zero. Then the reaction sample was placed in a constant temperature water bath (60.0 ± 0.1 °C) and the progress of the polymerization was followed by ^{1}H NMR.

Polymerization of one specific sample: 220 μL of $(TMP)Co^{II}\bullet$ (1.00×10^{-3} M in C_6D_6), 40 μL of AIBN (0.190 M in C_6D_6), and 190 μL of C_6D_6 were mixed in a vacuum-adapted NMR tube. 60 μL of vinyl acetate (VAc, $d = 0.932$ g/mL) was injected to this NMR tube and the resultant reaction solution was subjected to three freeze−pump−thaw cycles. ^{1}H NMR was run on the degassed sample and then the sample was placed in a 60.0 ± 0.1 °C water bath and the progress of polymerization was followed by ^{1}H NMR. The polymerization was stopped at each 10 min interval by immersing the sample in a 0 °C ice bath followed by ^{1}H NMR measurement at room temperature. After 120 min the solvent and unreacted monomers were removed by vacuum evacuation and the remaining polymer products were dissolved in THF for GPC analysis without further purification. Monomer conversion reached 4.36% in 120 min and the number averaged molecular weight of the polymeric products was 3340 with polydispersity of 1.16.

Analytical Techniques. Identification of $(TMP)Co^{II}\bullet$, organo-cobalt porphyrin complexes, and monomer conversion were evaluated by ^{1}H NMR at ambient temperature using a Bruker AC-360 spectrometer interfaced to an Aspect 300 computer. Chemical shifts were calibrated relative to solvent benzene peak at 7.155 ppm. The percent conversion of monomer was determined by comparing the integrations of the resonances corresponding to the vinyl protons of the monomer (3.9−4.9 ppm) and polymer (4.9−5.5 ppm).

Gel permeation chromatography (GPC) analysis for polymer products were performed on a Shimadzu modular system, comprised of a Polymer Laboratories 5.0 μm PLgel guard column (50 × 7.5 mm) followed by three linear PLgel columns (10^6, 10^4, and 5 ×

(48) Chrzastowski, J. Z.; Cooksey, C. J.; Johnson, M. D.; Lockman, B. L.; Steggles, P. N. *J. Am. Chem. Soc.* **1975**, *97*, 932–934.
(49) Dodd, D.; Johnson, M. D.; Lockman, B. L. *J. Am. Chem. Soc.* **1977**, *99*, 3664–3673.
(50) Endicott, J. F.; Balakrishnan, K. P.; Wong, C.-L. *J. Am. Chem. Soc.* **1980**, *102*, 5519–5526.
(51) Stolzenberg, A. M.; Cao, Y. *J. Am. Chem. Soc.* **2001**, *123*, 9078–9090.
(52) Goto, A.; Zushi, H.; Hirai, N.; Wakada, T.; Tsujii, Y.; Fukuda, T. *J. Am. Chem. Soc.* **2007**, *129*, 13347–13354.
(53) Yamago, S.; Kayahara, E.; Kotani, M.; Ray, B.; Kwak, Y.; Goto, A.; Fukuda, T. *Angew. Chem., Int. Ed.* **2007**, *46*, 1304–1306.
(54) Bakac, A.; Espenson, J. H. *J. Am. Chem. Soc.* **1986**, *108*, 719–723.
(55) Bakac, A.; Espenson, J. H. *Inorg. Chem.* **1989**, *28*, 4319–4322.
(56) Espenson, J. H.; Shimura, M.; Bakac, A. *Inorg. Chem.* **1982**, *21*, 2537–2542.
(57) Fukuda, T.; Ma, Y.-D.; Inagaki, H. *Macromolecules* **1985**, *18*, 17–26.
(58) Lindsey, J. S.; Wagner, R. W. *J. Org. Chem.* **1989**, *54*, 828–836.

10^2 Å) in an oven (CTO-10A), a UV detector (SPD-10AV) at 600 nm, and a differential refractive index detector (RID-10A). Tetrahydrofuran (THF) was used as the eluent at 40 °C with a flow rate of 1 mL min^{-1}. This system was calibrated using narrow peak width polystyrene standards (Easical, preprepared polymer calibrants purchased from Polymer Laboratories) ranging from 580 to 7.5 × 10^6 g mol^{-1}.

Kinetic Simulation. The kinetic simulations were conducted by using MacKinetics v0.9.1 and Micromath Scientist 2.01. A set of equations and rate constants from the decomposition of AIBN to give cyanoisopropyl radical to the degenerative radical interchange to form oligomer-cobalt complexes were used for the simulation. The rate constant for AIBN decomposition was calculated from tables provided by Wako Chemicals. The radical initiator efficiency ($k_d/(k_d + k_t)$) was approached by following the disappearance of (TMP)Co^{II}• during the induction period. The complete reaction scheme and the best set of rate constants found by the simulation are listed in the Supporting Information.

DFT Calculations. The geometry optimizations were carried out with the Turbomole program[59] coupled to the PQS Baker optimizer.[60] Geometries were fully optimized as minima or transition states at the BP86[61] level using the SV(P) basis set[62] on all atoms and small-core pseudopotential[63] on cobalt. Stationary points were characterized by vibrational analysis (numerical frequencies); ZPE and thermal corrections (entropy and enthalpy, 298 K, 1 bar) from these analyses are included. The free energies (kcal mol^{-1}) obtained by these procedures are reported in Scheme 4. The results of single point calculations at the b3-lyp level,[64] using the polarized triple-ζ TZVP basis[59] (small-core pseudopotential[59] on Co) are also included in Scheme 4. Optimized geometries of the species (por)Co, (por)Co-R_2 and (por)Co$(R_2)_2$ are supplied in the Supporting Information. The spin density plot shown in Figure 6 was generated with Molden.[65]

Acknowledgment. This work was supported by grant NSF-CHE-0501198 and The Netherlands Organization for Scientific Research (NWO-CW). We thank Prof. Peter H. M. Budzelaar for helpful discussions.

Supporting Information Available: Distributions of **1**, **3**, **4**, **5** at different conditions, DFT calculations for (por)Co^{II}, (por)Co$(R_2)_2$, kinetic simulations for a representative polymerization process (shown in Figure 5), and complete ref 59a. This material is available free of charge via the Internet at http://pubs.acs.org.

JA804010H

(59) (a) Ahlrichs, R.; et al. *Turbomole*, version 5; Theoretical Chemistry Group, University of Karlsruhe: Karlsruhe, Germany, January 2002. (b) Treutler, O.; Ahlrichs, R. *J. Chem. Phys.* **1995**, *102*, 346–354.
(60) (a) *PQS*, version 2.4; Parallel Quantum Solutions: Fayetteville, AR, 2001 (the Baker optimizer is available separately from PQS upon request. (b) Baker, J. *J. Comput. Chem.* **1986**, *7*, 385–395.
(61) (a) Becke, A. D. *Phys. Rev. A* **1988**, *38*, 3098–3100. (b) Perdew, J. P. *Phys. Rev. B* **1986**, *33*, 8822–8824.
(62) Schäfer, A.; Horn, H.; Ahlrichs, R. *J. Chem. Phys.* **1992**, *97*, 2571–2577.
(63) (a) Turbomole basisset library, Turbomole, version 5, see ref 59a. (b) Andrae, D.; Haeussermann, U.; Dolg, M.; Stoll, H.; Preuss, H. *Theor. Chim. Acta* **1990**, *77*, 123–141.
(64) (a) Lee, C.; Yang, W.; Parr, R. G. *Phys. Rev. B* **1988**, *37*, 785–789. (b) Becke, A. D. *J. Chem. Phys.* **1993**, *98*, 1372–1377. (c) Becke, A. D. *J. Chem. Phys.* **1993**, *98*, 5648–5652. (d) Calculations were performed using the Turbomole functional "b3 lyp", which is not identical to the Gaussian "B3LYP" functional.
(65) Schaftenaar, G.; Noordik, J. H. J. *Comput.-Aided Mol. Des.* **2000**, *14*, 123–134.